

Multiple bifurcations and local energy minimizers in thermoelastic martensitic transformations

Chen Xuan¹ · Shurong Ding¹ · Yongzhong Huo¹

Received: 14 February 2015 / Revised: 16 April 2015 / Accepted: 6 July 2015 / Published online: 23 September 2015

© The Chinese Society of Theoretical and Applied Mechanics; Institute of Mechanics, Chinese Academy of Sciences and Springer-Verlag Berlin Heidelberg 2015

Abstract Thermoelastic martensitic transformations in shape memory alloys can be modeled on the basis of nonlinear elastic theory. Microstructures of fine phase mixtures are local energy minimizers of the total energy. Using a one-dimensional effective model, we have shown that such microstructures are inhomogeneous solutions of the nonlinear Euler–Lagrange equation and can appear upon loading or unloading to certain critical conditions, the bifurcation conditions. A hybrid numerical method is utilized to calculate the inhomogeneous solutions with a large number of interfaces. The characteristics of the solutions are clarified by three parameters: the number of interfaces, the interface thickness, and the oscillating amplitude. Approximated analytical expressions are obtained for the interface and inhomogeneity energies through the numerical solutions.

Keywords Thermoelastic martensitic transformation · Microstructures · Nonlinear elasticity · Bifurcation · Energy minimizer

1 Introduction

Thermoelastic martensitic transformation (TEMT) is a type of solid–solid phase transition occurring in many shape memory alloys (SMAs) [1,2]. It is responsible for the shape

memory effect and pseudoelasticity, which are the two properties utilized in most applications of such alloys [3–8]. Microstructures of fine phase mixtures are often observed during the transformation, and they have a very strong effect on the macroscopic thermomechanical behavior of SMAs [9,10]. Many studies have been conducted in recent decades to determine when and which type of microstructures will appear during a given thermomechanical process [5,9–18].

Because TEMT takes place between two phases with different crystallographic structures, the primary driving force for the transformation is the bulk elastic strain energy difference of the two phases, the austenite, and the martensitic phase. However, owing to the diffusionless and thermoelastic nature of TEMT, both the interface energy and the inhomogeneous energy due to elastic constraints should play important roles in determining the observed microstructures of phase mixtures. It has been known for a long time [19] that the interface energy due to mismatches on the surface and interface boundaries has a strong effect on the nucleation and growth in many phase transitions. However, the constraint elastic energy accompanying the transformation is a rather special phenomenon of TEMT in SMAs [3]. For diffusion-controlled phase transitions, the constraint energy could be largely relaxed through atomic diffusions [20]. If the phase transition is diffusionless such as in TEMT, very strong elastic energies can be built up because of internal and external constraints due to dislocations, precipitates, grain boundaries, sample surfaces, and so on [3,5,21]. Thus, the microstructures of phase mixtures in TEMT must be analyzed by considering the interplay among the three contributions for the total energy, i.e., the bulk, the interfaces, and the constraint energy.

As indicated further by the hysteresis during TEMT, the microstructure is not unique under a given thermomechanical

Dedicated to Professor Zhongheng Guo.

✉ Yongzhong Huo
yzhuo@fudan.edu.cn

¹ Department of Mechanics and Engineering Science, Fudan University, Shanghai 200433, China

loading. Hence, they should be metastable states and local energy minimizers (LEMs) of the total energy. Their characteristics can be affected strongly by many factors, such as the rate of loading [22–25], the lattice orientation relative to the loading direction [26], the sample and grain sizes [27–29], and so on.

Owing to the metastability of such LEMs, it is generally very difficult to determine all possible solutions by analytical and numerical methods [14, 15]. Various effective one-dimensional nonlinear elastic models for slender SMA strips under uniaxial loading have been studied to understand the characteristics of the microstructures [30, 31]. Among them, the so-called foundation models have been studied most intensively in recent years [32–36]. Although local bifurcation analysis has shown that fine mixtures with a large number of interfaces could be LEMs of such foundation models [34, 35], solutions of large interface numbers are very difficult to obtain even numerically because of the high nonlinearity of the problem. Thus, still very little is known about the characteristics of such solutions of fine phase mixtures.

Attempts have been made to obtain such solutions through dynamic processes [36–38] by adding viscosity terms to the equations. However, it is not possible to obtain all possible LEMs through the dynamic process, and the role of viscosity is not clear for metallic materials. Asymptotic series solutions were proposed by the present authors in Ref. [39] using the homotopy analysis method (HAM) [40, 41]. It was shown that asymptotic solutions with a large number of interfaces could be obtained by HAM. However, the convergence of such solutions is not guaranteed.

Thus, we shall propose a hybrid method to combine HAM with the finite difference method (FDM) to obtain inhomogeneous solutions of the nonlinear Euler–Lagrange equation of the one-dimensional foundation model. Then the characteristics of such solutions will be studied in some detail. The results can be helpful in understanding the governing mechanism of fine phase mixtures in thermoelastic martensitic transformation.

The paper is organized as follows. In the next section, the nonlinear elastic model of TEMT will be introduced briefly. Then the approximated one-dimensional foundation model is presented. The hybrid HAM–FDM method is proposed to obtain the numerical solutions of fine phase mixtures. In Sect. 3, the bifurcation condition for the existence of such inhomogeneous solutions of fine phase mixtures is obtained. The effect of loading and model parameters on bifurcation behavior is discussed. Multiple bifurcations under loading leads to the possibility of microstructure evolutions. In Sect. 4, numerical solutions of fine phase mixtures are obtained by the hybrid HAM–FDM method for various loading conditions and different model parameters. Some typical features of the solutions are taken as the characteristics for the microstructures. That is, three quantities—the interface

number, the interface thickness, and the strain oscillating amplitude—are considered as the determining characteristics. Our numerical simulations confirmed that both the interface energy and the constraint energy are determined completely by these three quantities. The final conclusion is given in the last section.

2 Nonlinear elastic models and the hybrid numerical method

First, the nonlinear elastic model for TEMT will be reviewed briefly, and then the one-dimensional approximation of a foundation model will be presented. Then the hybrid method for numerical solutions will be introduced.

2.1 Nonlinear elastic model for martensitic transformations

TEMT takes place diffusionlessly between two phases with rather different crystallographic structures and is accompanied by large shear strains. That is, the deformation gradients of the martensite \mathbf{F}_M and the austenite \mathbf{F}_A are related by [2, 5]

$$\mathbf{F}_M = \mathbf{F}_A + \mathbf{d} \otimes \mathbf{p}, \quad (1)$$

where the unit vector \mathbf{p} is the normal of the interface between the two phases, called the habit plane. The vector \mathbf{d} is perpendicular to \mathbf{p} and represents the shear. When the lattice structures of the two phases are known, the shear strain can be calculated according to the Wechsler–Lieberman–Read method [42] or, equivalently, Bowles–Mackenzie method [43]. Both experimental and theoretical studies have confirmed that the TEMTs in SMA can be well described by macroscopic deformation gradients (1) without having to introduce other order parameters of a microscopic nature [2, 5]. Moreover, the bulk Helmholtz free energy would be just a function of the deformation gradient at a given temperature, just like thermoelastic materials [44]. Thus, for a body B the total energy would be

$$E_t = E_b = \int_B W(\nabla \mathbf{u}, T) dV, \quad (2)$$

where $\nabla \mathbf{u} = \mathbf{F} - \mathbf{I}$ is the displacement gradient and W is the nonlinear elastic strain energy density. At relatively high temperatures where only the parent phase can exist, the elastic strain energy is convex in strain with the minimum at $\mathbf{F} = \mathbf{F}_A$, just like regular elastic materials. However, W will become nonconvex and can have more than one minimum at temperatures where both phases can coexist. Moreover, 24 different variants of martensite can often appear owing to the lattice symmetries, even for single-crystal SMAs. Thus, W

would have 24 equal-height martensitic minimums in addition to that of austenite.

Because of the nonconvexity of the strain energy W , the total energy minimizer of Eq. (2) is generally not unique, and microstructures of fine phase mixtures can appear as LEMs [9, 45]. Thus, during a TEMT under thermomechanical loading, the austenite phase that was previously the unique global energy minimizer becomes unstable, and the new phase, the martensitic phase, will nucleate in the austenitic matrix. Microstructures as mixtures of austenite and martensitic variants will appear as metastable LEMs. Hence, this is a kind of bifurcation from the unique stable solution of austenite to nonunique metastable solutions of phase mixtures.

For a phase mixture, there exist large lattice distortions near the interfaces between the two phases of very different lattice structures. Thus, an interface energy of a strain gradient type could be added to Eq. (2) as

$$E_t = E_{\text{bulk}} + E_{\text{int}} = \int_B (W(\nabla u, T) + k(\nabla \nabla u, T)) dV. \quad (3)$$

However, very few useful results have been obtained for the two- and three-dimensional models because of the mathematical and numerical difficulties of considering a large number of different martensitic variants [9, 11, 14, 15, 46]. Thus, various one-dimensional approximated models have been proposed and studied analytically and numerically. We shall consider here the so-called foundation model.

2.2 One-dimensional foundation model

By considering slender strips of single-crystal SMAs in uniaxial loading experiments, only one favorable martensitic variant is usually picked out by the applied uniaxial stress. Thus, the problem is reduced to considering only a two-well nonconvex elastic strain energy function with interfaces of the austenite and the favored martensitic variant [30]. It was shown in Ref. [31] that the one-dimensional approximation of Eq. (3) would lead a unique phase mixture with only one interface. To model fine phase mixtures observed in many experiments, various effective one-dimensional models have been proposed to consider constraints imposed by the boundary and surrounding matrix, such as the so-called foundation models [32–36].

The one-dimensional foundation model proposed first by Ref. [35] is based on the following total free energy for a slender bar:

$$E_t = E_{\text{bulk}} + E_{\text{int}} + E_{\text{inh}} = \int_0^L \left[W(u_x(x)) + \alpha u_{xx}^2(x) + \beta (u(x) - u_H(x))^2 \right] dx, \quad (4)$$

where L is the length of the bar; and $u(x)$, $u_x(x)$, and $u_{xx}(x)$ are the displacement, the strain, and the strain gradient, respectively. The elastic strain energy density $W(u_x)$ is a nonconvex double-well function with its two minimums representing the austenite and martensite. The interface energy E_{int} is proportional to the square of the strain gradient and penalizes the phase boundaries. The coefficient of interfacial energy (CIFE) α is a positive constant. The inhomogeneity energy E_{inh} was originally proposed as an artificial pseudo-rigid foundation in Ref. [35] to mimic the elastic constraints of the boundaries and the surrounding matrix in three dimensions. $u_H(x)$ is taken as the homogenous displacement of an elastic foundation bar under the same boundary conditions. That is, if we consider the displacement controlled boundary condition

$$u(0) = u_0, u(L) = u_0 + dL \text{ and } u_{xx}(0) = u_{xx}(L) = 0, \quad (5)$$

with u_0 a constant and $d = (u(L) - u(0))/L$ the engineering strain, the homogeneous displacement is

$$u_H(x) = (u(L) - u(0))x/L + u(0) = u_0 + dx. \quad (6)$$

As discussed in Refs. [35] and [47], this term penalizes inhomogeneous solutions with the positive constant β as the coefficient of inhomogeneous energy (CIHE).

Compared to the more popular elastic foundation model of which the last term in Eq. (4) is taken as being proportional to u^2 , the energy functional (4) is translation-invariant. That is, the translation u_0 in the boundary condition (5) does not affect E_t of Eq. (4) but would have a large effect if E_{inh} is assumed to be proportional to u^2 as in the elastic foundation model. In the model proposed by Dai and Cai in Ref. [48], the effect of the constraints is considered by including an additional equation for the vertical displacement. However, they considered only polycrystalline SMAs with just two interfaces during the TEMT.

The Euler–Lagrange equation for the minimization of the total free energy (4) under the boundary condition is the following fourth-order nonlinear ordinary differential equation (ODE):

$$G_{\text{eff}}(u_x)u_{xx} - 2\alpha u_{xxxx} - 2\beta(u - u_H) = 0, \quad (7)$$

with the effective modulus G_{eff} defined as the curvature of the potential energy $W(u_x)$,

$$G_{\text{eff}}(u_x) = W_{\varepsilon\varepsilon}(u_x). \quad (8)$$

It is strictly positive for elastic materials with convex elastic strain energy W . Thus, Eq. (7) with the boundary condition (5) has a unique trivial solution, $u = u_H$, even for $\alpha = \beta = 0$, which is a homogeneous deformation by Eq. (6).

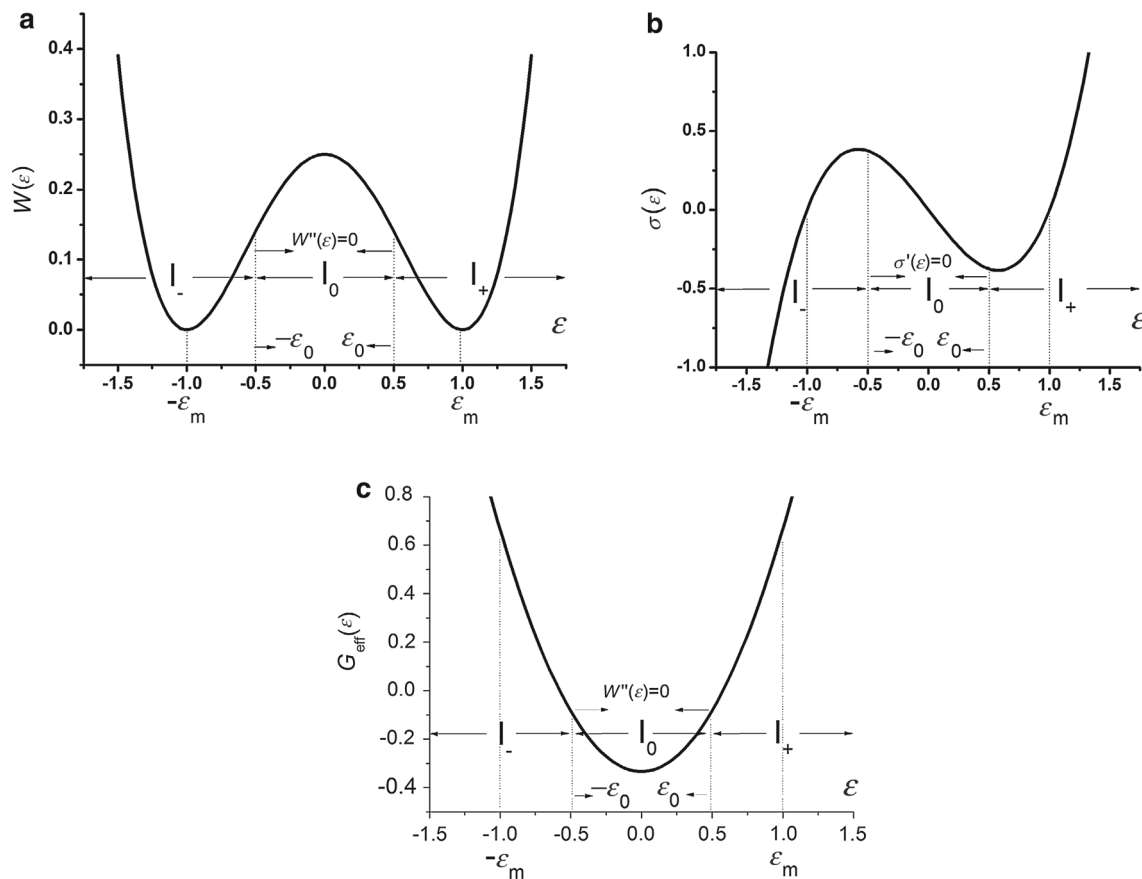


Fig. 1 Nonconvex elastic potential function. **a** The two well potential $W(\varepsilon)$. **b** The nonmonotonic stress–strain relation $\sigma = W'(\varepsilon)$. **c** The effective modulus with negative part $G_{\text{eff}} = W''(\varepsilon)$

However, the uniqueness will be lost if the effective modulus G_{eff} can become zero and even negative in the case where $W(\varepsilon)$ is nonconvex for materials under phase transitions. For example, consider the following potential function and its effective modulus:

$$W(\varepsilon) = E(\varepsilon^2 - 1)^2/4, \tag{9}$$

$$G_{\text{eff}}(\varepsilon) = 3E(\varepsilon^2 - 1/3). \tag{10}$$

As shown in Fig. 1, W is nonconvex with two minimums at $\varepsilon_m^\pm = \pm 1$ (Fig. 1a), with a nonmonotonic stress–strain diagram (Fig. 1b), and G_{eff} is zero at the two inflection points $\pm\varepsilon_0 = \pm 1/\sqrt{3}$ and is negative in between $(-\varepsilon_0, \varepsilon_0)$, where W is concave (Fig. 1c). Then it is possible to obtain nontrivial inhomogeneous solutions of Eq. (7) in addition to the trivial one $u = u_H$.

By Eq. (4), the free energy of the trivial homogeneous solution is simply $E_t = W(d)L$. According to Eq. (9), it is the energy minimizer when $d = \pm\varepsilon_m = \pm 1$. As the strain d moves away from the two minimums, the energy increases, and eventually the homogeneous solution could

become unstable in the concave region $d \in (-\varepsilon_0, \varepsilon_0)$. Then inhomogeneous solutions of Eq. (7) would appear as the LEMs of the total free energy (4), a kind of bifurcation [35,39,47].

As shown in Fig. 2, the LEMs are nonmonotonic solutions $u(x)$, with the strain $u_x(x)$ oscillating between the two energy wells. Thus, they can be characterized by the total number of points $\{x_i, i = 1, 2, \dots, k\}$ satisfying $u_x(x_i) = d$, for example, $k = 5$ for Fig. 2b. This corresponds to the number of oscillations and should be identified as the number of interfaces between the two phases. The solutions can be further characterized by the oscillating amplitude $2A > 0$ and the thickness of the interfaces $t > 0$, as shown in Fig. 2b. For the trivial homogeneous solution $u(x) = u_H(x)$, we set $k = A = t = 0$. Therefore, bifurcation is from a solution with $k = A = t = 0$ to solutions with $k, A, t > 0$. The condition for the existence of nontrivial solutions will be given in the next section. Here we shall first rewrite our equations in dimensionless forms and introduce the hybrid numerical method to calculate such solutions.

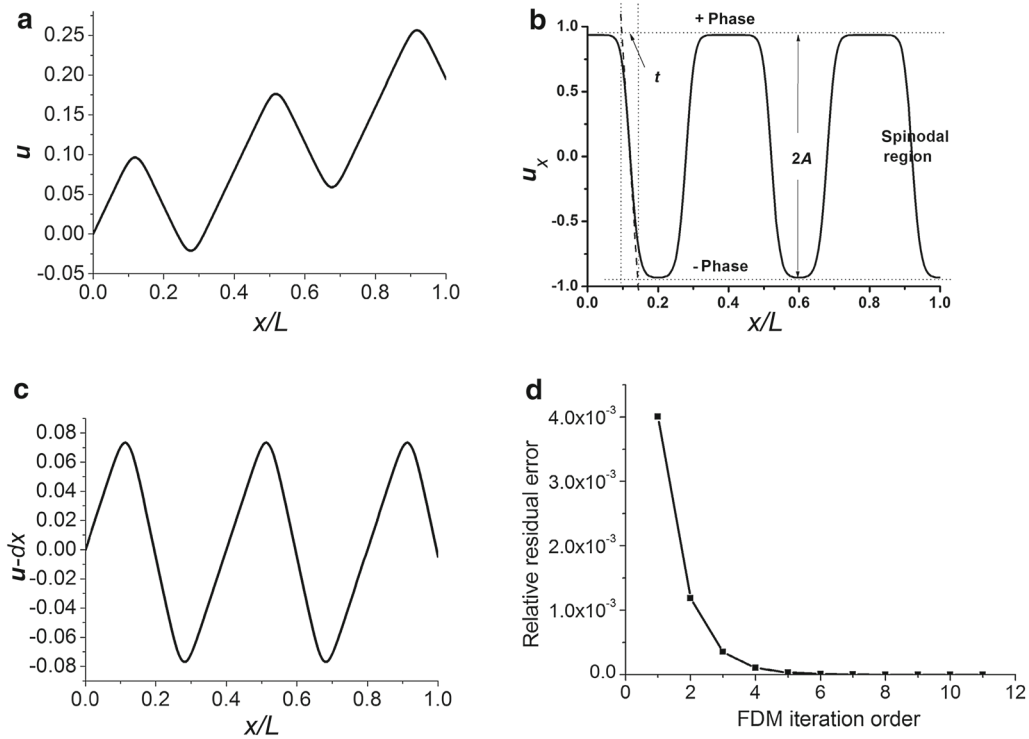


Fig. 2 Inhomogeneous solution of the Euler-Lagrange equation. **a** The displacement $u(x)$. **b** The strain $u_x(x)$. **c** The scaled displacement $v(x/L)$. **d** Relative residual error against iteration orders

2.3 The hybrid HAM–FDM method

The dimensionless versions of Eqs. (4)–(10) read as follows

$$\xi = x/L, \quad v(\xi) = (u(x) - u_H(x))/L, \quad \hat{\alpha} = \alpha/(EL^2), \quad \hat{\beta} = \beta L^2/E, \tag{11}$$

$$\hat{W}(\varepsilon) = (\varepsilon^2 - 1)^2/4 \text{ and } \hat{G}_{\text{eff}}(\varepsilon) = 3(\varepsilon^2 - 1/3), \tag{12}$$

$$e_t = \frac{E_t}{EL} = \int_0^1 \left[\hat{W}(v_\xi(\xi) + d) + \hat{\alpha}v_{\xi\xi}^2(\xi) + \hat{\beta}v^2(\xi) \right] d\xi, \tag{13}$$

$$\hat{G}_{\text{eff}}(v_\xi + d)v_{\xi\xi} - 2\hat{\alpha}v_{\xi\xi\xi\xi} - 2\hat{\beta}v = 0, \tag{14}$$

$$v(0) = v(1) = 0, \text{ and } v_{xx}(0) = v_{xx}(1) = 0. \tag{15}$$

It is generally not possible to find analytical solutions of the highly nonlinear fourth-order ODE (14) with the boundary conditions (15). The finite difference method (FDM) is often applied together with the Newton iteration method (NIM) [37,38,49] to obtain the numerical solutions. The numerical scheme is

$$\mathbf{v}^{(n+1)} = \mathbf{v}^{(n)} - \left[\frac{\partial \mathbf{g}(\mathbf{v})}{\partial \mathbf{v}^{(n)}} \right]^{-1} \cdot \mathbf{g}(\mathbf{v}^{(n)}), \tag{16}$$

for the $(n + 1)$ th-order solution $\mathbf{v}^{(n+1)}$, with

$$g_i(\mathbf{u}) = \frac{1}{\Delta x} \left[W' \left(\frac{u_{i+1} - u_i}{\Delta x} \right) - W' \left(\frac{u_i - u_{i-1}}{\Delta x} \right) \right]$$

$$\begin{aligned} & -2 \frac{\alpha}{\Delta x^4} (u_{i+2} - 4u_{i+1} + 6u_i - 4u_{i-1} + u_{i-2}) \\ & - 2\beta(u_i - u_H). \end{aligned} \tag{17}$$

For the Newton iteration to be effective, it is very important to have an initial guess $\mathbf{v}^{(0)}$ not very far from the final solution. This can be rather difficult for inhomogeneous solutions with a very large interface number k . Very often, solutions with k no more than 5 are studied. For higher k 's, we need more effective methods.

As proposed in Ref. [39], HAM can be applied to obtain the asymptotic series solutions of Eq. (14) with boundary conditions (15). The asymptotic solutions with a given interface number k read

$$v_N(\xi) = \sum_{i=0}^N b(i, N) \hbar^i \sin(2i + 1)k\pi\xi, \tag{18}$$

where \hbar is an auxiliary parameter used in HAM to control the convergence of the solution for large N . The coefficients $b(i, N), i = 1, 2, 3, \dots, N$ must be calculated iteratively. Note that Eq. (18) is not a Fourier series expansion because $b(i, N)$ does not denote the Fourier coefficients and must be recalculated for every cutoff N .

As shown in Ref. [39], it is possible to obtain the bifurcation condition and the nontrivial asymptotic solutions for a large number of k by this method. Moreover, the solutions

(18) converge numerically to some functions, with their strain oscillating between the two energy wells like those shown in Fig. 2.

However, there is no mathematical proof of convergence for HAM. Thus, it would be extremely useful to check the solutions using different methods. We propose the following hybrid procedure to obtain the numerical solutions with a given interface number k :

- (1) HAM solution (18) is calculated to a sufficiently large order N to ensure good approximation.
- (2) The HAM solution is inserted into Eq. (16) as the initial guess $\mathbf{v}^{(0)}$ to start the iteration by NIM with the FDM of Eq. (17).

The solution shown in Fig. 2 is obtained by this method with a HAM solution (18) of $N = 30$. Usually, rather good accuracy is obtained after just a very small number of iterations. The relative residual errors of Eq. (14) as a function of the FDM iteration orders are shown in Fig. 2d. One can see that the iteration in which a high-order HAM solution is used as the initial solution for the FDM converges rather quickly.

It is obvious from Fig. 2 that the inhomogeneous solutions of Eq. (7) all have their strains u_x oscillating between the two wells of the potential energy (9). However, many solutions can exist for a given engineering strain d , and they can have very different interface numbers k , amplitudes A , and interface thicknesses t . It is clear that not all of them can be the absolute minimizers of the total free energy (4). They are simply the LEMs, i.e., the solutions of the Euler–Lagrange equation (4) with the boundary condition (5). These LEMs are metastable and are very useful for understanding the martensitic transformations, in particular the hysteresis. Thus, their characteristics will be studied in some detail in what follows. First, the condition for the existence of such inhomogeneous solutions must be established.

3 Bifurcation conditions for local energy minimizers

The bifurcation condition for the existence of LEMs can be obtained either by local bifurcation analysis [35] or through HAM [39]. The result is summarized here first. Then the bifurcations during the loading–unloading process are discussed in detail.

3.1 Bifurcation conditions and region of local energy minimizers

First, the necessary condition for the existence of LEMs, i.e., inhomogeneous solutions of Eqs. (14) and (15), with the interface number $k > 0$ at a given strain d , are obtained [35, 39] as

$$k_-(d) < k < k_+(d), \tag{19}$$

where $k_{\pm}(d)$ are two functions defined as

$$k_{\pm}(d) = \frac{\kappa}{\sqrt{\delta}\varepsilon_0} \left[\varepsilon_0^2 - d^2 \pm ((\hat{\alpha}_\delta^2 - d^2)(\varepsilon_\delta^2 - d^2 + 2\delta\varepsilon_0^2))^{1/2} \right]^{1/2}, \tag{20}$$

with the constants

$$\varepsilon_\delta = \varepsilon_0\sqrt{1 - \delta}, \quad \delta = 4\sqrt{\hat{\alpha}\hat{\beta}}, \quad \kappa = (\hat{\beta}/\hat{\alpha})^{1/4} / \pi. \tag{21}$$

As shown in Fig. 3a, condition (19) is satisfied by (d, k) in the following region with its upper and lower boundaries given by (20)

$$\Omega_{\text{LEM}s} = \{(d, k) \mid -\varepsilon_\delta < d < \varepsilon_\delta, k_-(d) < k < k_+(d)\}. \tag{22}$$

Thus, we may call $\Omega_{\text{LEM}s}$ the region of LEMs. As shown in Fig. 3, $\Omega_{\text{LEM}s}$ is convex in the (d, k) plane and symmetric in strain because we used a symmetric potential function (9). At $d = 0$, we have a maximal $k_+(0)$ and minimal $k_-(0)$ as

$$k_{\pm}(0) = \frac{\kappa}{\sqrt{\delta}} \sqrt{1 \pm \sqrt{1 - \delta^2}}. \tag{23}$$

It is obvious from Eq. (20) that the region $\Omega_{\text{LEM}s}$ will be simply shifted up for larger κ , as shown in Fig. 3a. Hence, LEMs would generally have larger numbers of interfaces for larger κ . The constant δ must satisfy $0 < \delta < 1$ to ensure the existence of such a region by Eq. (21). $\Omega_{\text{LEM}s}$ is bigger for smaller δ as shown clearly in Fig. 3b.

The exact bifurcation condition for the appearance of LEMs is more involved because the interface number k must be a positive integer. Moreover, multiple bifurcations to various LEMs can occur upon loading–unloading processes. We shall first consider the primary bifurcation to LEMs by loading the sample from the left minimum of the strain energy function W given by Eq. (9), i.e., $d_0 = -\varepsilon_m = -1$. The situation is symmetric for unloading from the right minimum owing to the symmetry of W .

3.2 Primary bifurcation to LEMs

The homogeneous trivial solution, $v = 0 (u = u_H)$, is and will remain the unique solution of Eqs. (14) and (15) until d increases to $d = -\varepsilon_\delta$, with $k_{\pm}(-\varepsilon_\delta) = \kappa$. This is the leftmost boundary point of the solution region $\Omega_{\text{LEM}s}$ and is slightly larger than the inflection strain $-\varepsilon_0$ by Eq. (21). The situation will be very different for different values of the constant κ of Eq. (21).

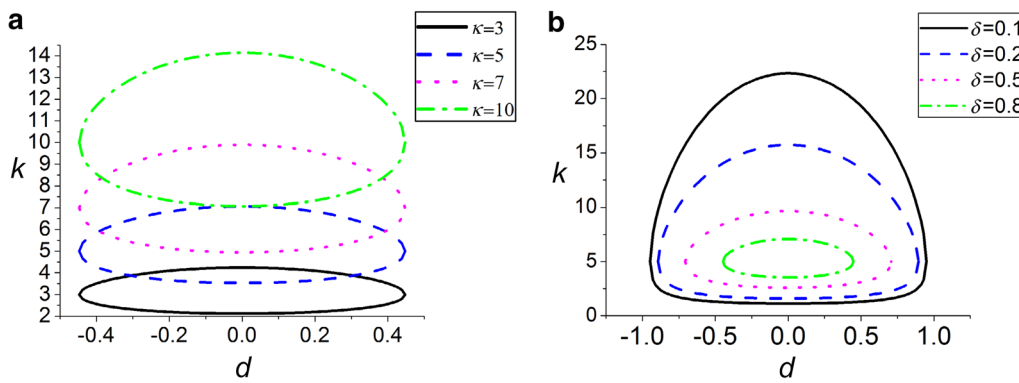


Fig. 3 Region of local energy minimizers Ω_{LEMs} for **a** different κ 's and **b** different δ 's.

If κ is a positive integer, $\kappa = n$, an inhomogeneous solution of Eqs. (14) and (15) with the interface number $k_c = k_{\pm}(-\varepsilon_{\delta}) = n$ would be possible upon further loading. Thus, a bifurcation from one trivial solution with $k = 0$ to two solutions with $k = 0$ and $k = n$ would have occurred at $d = -\varepsilon_c^0 = -\varepsilon_{\delta}$, as shown in Fig. 4a.

However, if $\kappa > 0$ is not an integer, then the bifurcation must wait until the loading has reached a critical strain $d = -\varepsilon_c^0$ as

$$\varepsilon_c^0 = \varepsilon_0 \sqrt{1 - \delta / \delta_c(\kappa)}, \tag{24}$$

where the function $\delta_c(\kappa)$ is positive and defined as

$$\delta_c(\kappa) = \begin{cases} \phi(\lfloor \kappa \rfloor / \kappa), & \kappa \leq \kappa_m, \\ \phi(\lceil \kappa \rceil / \kappa), & \kappa > \kappa_m, \end{cases} \tag{25}$$

where $\lceil \kappa \rceil$ and $\lfloor \kappa \rfloor$ are the ceiling and floor functions, i.e., the smallest integer no less than κ and the largest integer no larger than κ , respectively. That is, we would always have $\lfloor \kappa \rfloor \leq \kappa \leq \lceil \kappa \rceil$. The function $\phi(x) \geq 0$ and the geometric mean value $\kappa_m \geq 0$ are defined as

$$\phi(x) = 2x^2 / (1 + x^4) \text{ and } \kappa_m = \sqrt{\lfloor \kappa \rfloor \lceil \kappa \rceil}. \tag{26}$$

As shown in Fig. 5a, $\delta_c(\kappa)$ is a piecewise monotonic function with maximum $\delta_c(n) = 1$ at the positive integer n . It increases in the intervals $(0, 1]$ and $(\sqrt{n(n-1)}, n]$ and decreases in $(n, \sqrt{n(n+1)}]$. For large κ , it approaches 1.

Thus, by Eq. (24), the first bifurcation to inhomogeneous LEMs would occur at $d = -\varepsilon_c^0$ when the two positive constants δ and κ of Eq. (21) satisfy the condition

$$\delta < \delta_c(\kappa). \tag{27}$$

As depicted in Fig. 5b, the critical strain ε_c^0 of Eq. (24) is also a piecewise monotonic function of κ , rather similar to $\delta_c(\kappa)$. However, larger δ will result in smaller ε_c^0 .

The number of interfaces of the LEMs at the primary bifurcation is given as

$$k = k_c(\kappa) = \begin{cases} \lfloor \kappa \rfloor, & \kappa < \kappa_m, \\ \lceil \kappa \rceil, & \kappa > \kappa_m, \\ \lfloor \kappa \rfloor \text{ and } \lceil \kappa \rceil, & \kappa = \kappa_m, \end{cases} \tag{28}$$

Thus, when the positive constant κ is not an integer, three different situations are possible at the primary bifurcation $d = -\varepsilon_c^0$. That is, we can have one LEM with the interface number $k_c = \lfloor \kappa \rfloor < \kappa < \kappa_m$ as shown in Fig 4b, one LEM with $k_c = \lceil \kappa \rceil > \kappa > \kappa_m$ as in Fig 4c, and two LEMs with $k_c^1 = \lfloor \kappa \rfloor$ and $k_c^2 = \lceil \kappa \rceil$ for $\kappa = \kappa_m$ as in Fig 4d. As shown in Fig. 5d, the interface number k_c of Eq. (28) is a step function of κ , with jumps from n to $n + 1$ at $n_m = \sqrt{n(n + 1)}$ for any positive integer n .

3.3 Subsequent bifurcations upon further loading

Following the primary bifurcation at $d = -\varepsilon_c^0$, further loading could result in more inhomogeneous LEMs with an interface number k other than k_c because the function $k_{-}(d)$ is decreasing and $k_{+}(d)$ is increasing for $d < 0$ according to Eq. (20) and Fig. 3. The critical strain $d = -\varepsilon_c(k)$ for such a solution with interface number k can be obtained by the condition $k = k_{-}(d)$ or $k = k_{+}(d)$. By Eq. (20), we have

$$\varepsilon_c(k) = \varepsilon_0 \sqrt{1 - \delta / \phi(k/\kappa)}. \tag{29}$$

Obviously, it recovers Eq. (24) for $k = k_c$ of Eq. (28). The admissible number of interfaces is given by the condition $\delta < \phi(k/\kappa)$, which is essentially

$$k_{-}(0) < k < k_{+}(0), \tag{30}$$

with $k_{\pm}(0)$ given by Eq. (23) the most upper and lower points of the region Ω_{LEMs} . As shown in Fig. 6a, with δ from 0 to 1, $k_{-}(0)$ is increasing from 0 to κ , but $k_{+}(0)$ is decreasing from infinity to κ . Both are shifted up by increasing κ . Given the

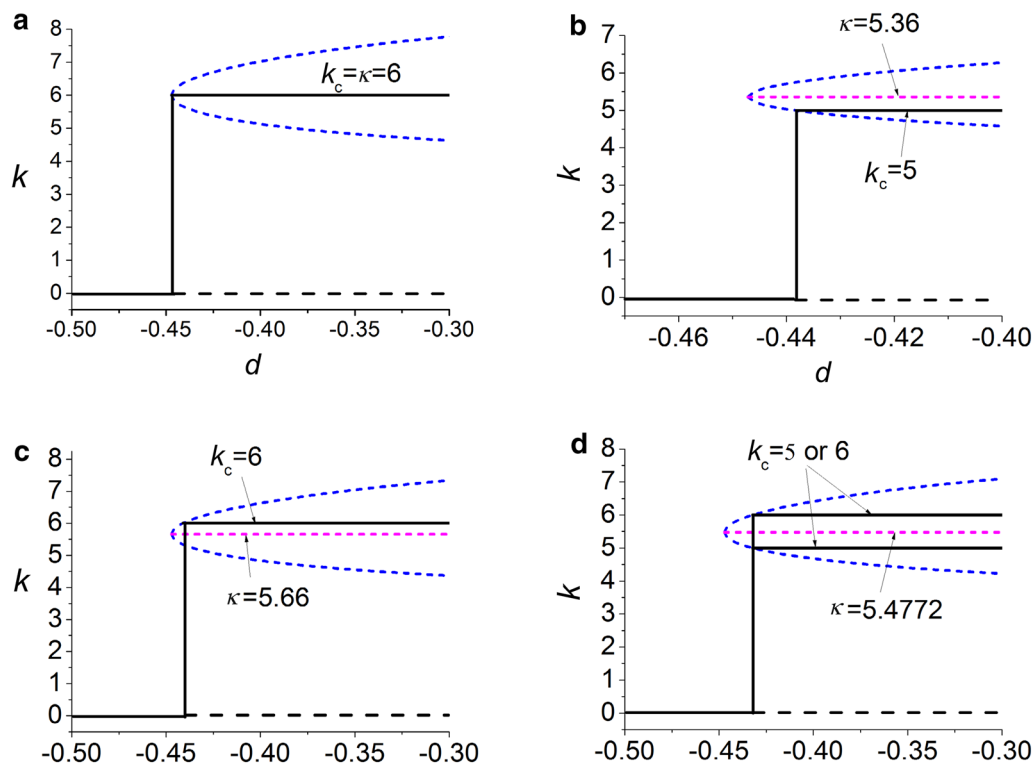


Fig. 4 Primary bifurcation for different values of the parameter κ . **a** $\kappa = n$. **b** $\kappa < \kappa_m$. **c** $\kappa > \kappa_m$. **d** $\kappa = \kappa_m$

two constants, all positive integers between the two curves are possible interface numbers of some inhomogeneous LEMs for loadings $-\varepsilon_c(k) < d < \varepsilon_c(k)$. Figure 6b depicts an example with $k = 1, 2, 3, 4$ all admissible interface numbers, as indicated by the horizontal lines. The critical $k_c = 2$ is achieved first and followed by further bifurcations to $k = 1, 3$, and 4 at the corresponding strains $d = \pm\varepsilon_c(k)$, indicated by circles and dashed vertical lines in Fig. 6b.

Before we study the characteristics of LEMs in the next sections, we would like to make two remarks regarding the difference between the primary and the subsequent bifurcations. First, the subsequent bifurcations are from inhomogeneous LEMs to solutions of the same type, while the primary bifurcation is from the homogeneous solution to inhomogeneous LEMs. Second, the homogeneous solution has lost its stability at the primary bifurcation, but the LEMs remain locally stable when more such solutions appear.

4 Characteristics of local energy minimizers

Inhomogeneous solutions of Eqs. (14) and (15) can be obtained using the hybrid method proposed in Sect. 2. That is, for given positive integer k and strain d satisfying the bifurcation condition (19), the HAM solution (18) is calculated to $N = 30$. Then it is inserted into Eq. (16) as $\mathbf{v}^{(0)}$ to start NIM with the FDM (17).

Figure 7 depicts some examples of such solutions. The relevant parameters (11) are chosen as $\hat{\alpha} = 1.5 \times 10^{-4}$ and $\hat{\beta} = 15$. By Eq. (21), we have $\delta = 0.19$ and $\kappa = 5.66$, satisfying condition (27). By Eqs. (24) and (28), the critical strain of the primary bifurcation is $\varepsilon_c^0 = 0.519$ and the critical interface number is $k_c = 6$. By Eq. (23), we find that the maximal admissible interface number is $k_M = 18$ and the minimal one is $k_m = 2$.

The solution with $k = k_c$ is shown in Fig. 7a with three different loading strains. Because d just entered the bifurcation region, $d = -0.517$, close to the critical strain $-\varepsilon_c^0 = -0.519$, the solution has a very small amplitude A and very large interface thickness t . As the loading proceeds, A increases and t decreases with d . The solution has a maximal A and minimal t at $d = 0$. Figure 7b–d depicts similar behavior for solutions with $k = 5, 2$, and 18 . As shown more clearly by Fig. 8, the amplitude A is small near $\pm\varepsilon_c(k)$ of Eq. (29) and has its maximum at $d = 0$. The thickness t is the reverse.

At $d = 0$, both the amplitude A and the total interface thickness t can be rather different for solutions with different interface numbers, as depicted in Fig. 8. It seems that the solutions with $k = k_m$ and $k = k_M$, as in Fig. 7c, d, have much smaller A and larger t than others, as in Fig. 7a, b.

From the viewpoint of the microstructures of martensitic transformations, the inhomogeneous LEMs with large A and small t , for example, Fig. 7a, b at $d = 0$, would

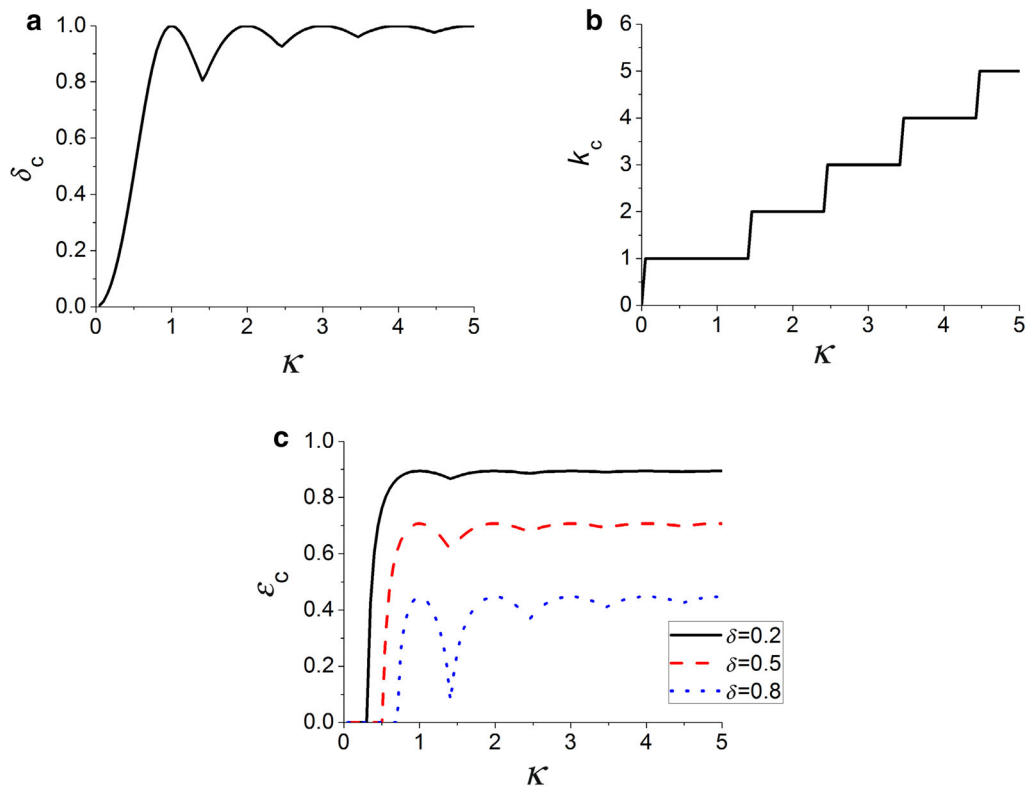


Fig. 5 Critical conditions at primary bifurcation. **a** Admissible condition $\delta < \delta_c(\kappa)$. **b** Critical interface number. **c** Critical strain

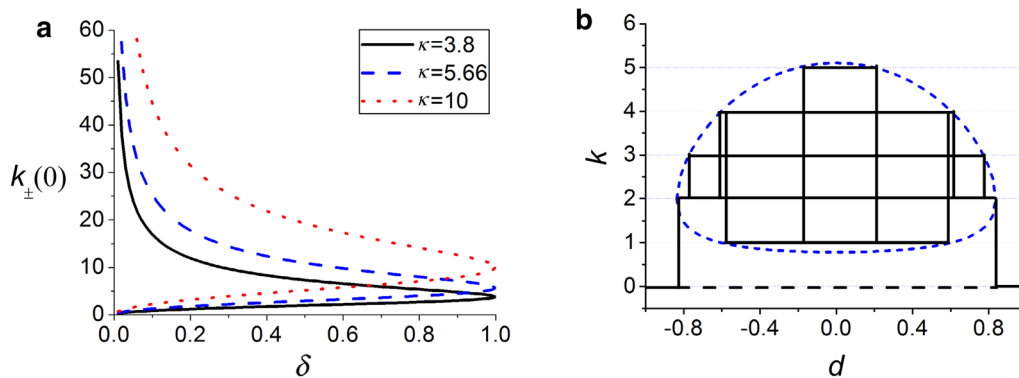


Fig. 6 Subsequent bifurcations. **a** Maximal and minimal number of interfaces. **b** Example of four further bifurcations

represent samples with alternative phases composed of fully developed phase bands with narrow interfacial boundaries in between. Other cases with smaller A and larger t would indicate distorted phase regions with indistinct interfaces. It is the competition of the different energy contributions for the total energy (4) that will decide which microstructures of LEMs are to be selected in a real situation. We calculate the energies, in particular the interface and inhomogeneity energies, in Eq. (4) or Eq. (13).

By Eq. (13), the dimensionless interface energy e_{int} should be proportional to the constant $\hat{\alpha}$ and the energy-penalizing inhomogeneity e_{inh} should be proportional to the constant $\hat{\beta}$.

Figure 9 depicts the results from our simulations obtained with various admissible strains d and interface numbers k for a number of pairs of parameters $\hat{\alpha}$ and $\hat{\beta}$. They seem to confirm such linear relations as

$$e_{\text{int}} = C_1 kt \left(\frac{A}{t}\right)^2 \hat{\alpha}, \tag{31}$$

$$e_{\text{inh}} = \frac{C_2}{\pi^2} \left[1 + \left(\frac{\pi}{2} - 1\right) \cos \frac{\pi kt}{2}\right]^2 \left(\frac{A}{k}\right)^2 \hat{\beta}, \tag{32}$$

with the constants $C_1 = 2.9$ and $C_2 = 0.287$. Note that the amplitude–interface thickness ratio, A/t , characterizes the

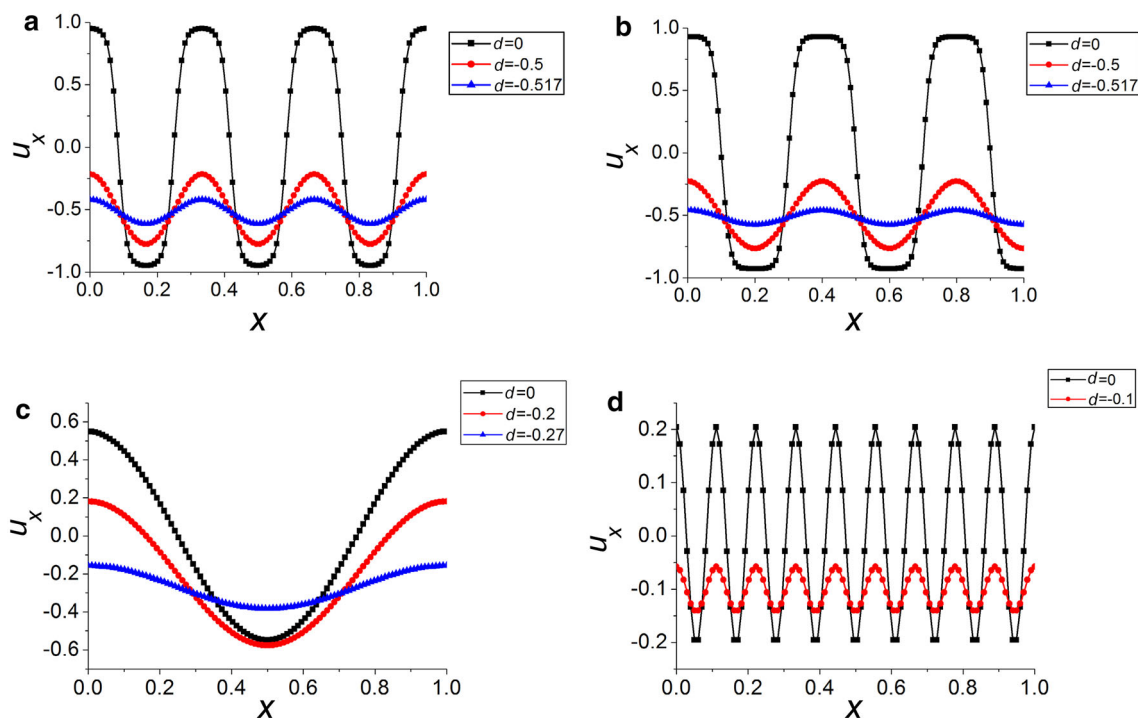


Fig. 7 Inhomogeneous solutions with various interface numbers. **a** $k = 6$. **b** $k = 5$. **c** $k = 2$. **d** $k = 18$

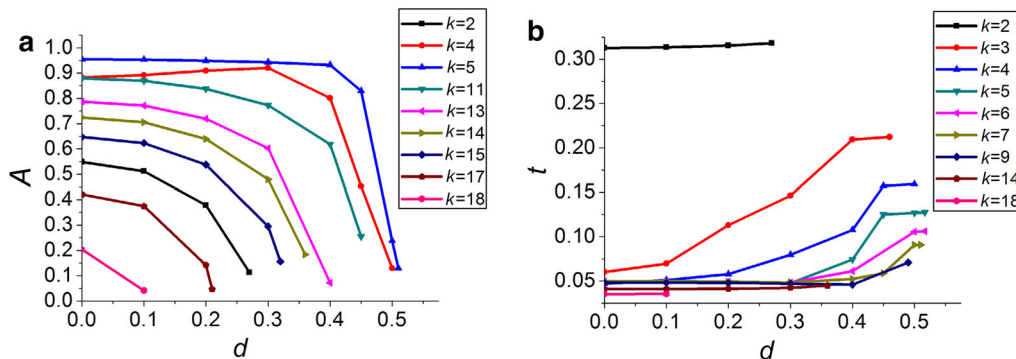


Fig. 8 Characteristics of inhomogeneous solutions with different interface numbers and at various loadings. **a** Amplitudes. **b** Interface thicknesses

strain gradient at the interface boundaries. The amplitude–interface number ratio A/k characterizes the amplitude of the displacement $v(\xi)$, as clearly indicated by the HAM solution (19).

The interface energy (31) seems to be proportional to the interface number k with the proportional coefficient $e_{\text{int}}^0 = C_1 t (A/t)^2 \hat{\alpha}$ as the interface energy of one interface. Such a linear relation of the interface energy has been used in many models of TEMTs and was previously derived through minimizations [32,36,47]. However, our numerical results in Figs. 7 and 8 show clearly that the coefficient $e_{\text{int}}^0 = C_1 t (A/t)^2 \hat{\alpha}$ is generally not a constant but varies with the loading, the parameters, and even the interface number itself.

Comparing Eq. (32) with Eq. (31), the inhomogeneity energy e_{inh} has a very different relation to the interface number k because it depends on the displacement $v(\xi)$ instead of the strain, according to Eq. (13). The proportionality to $1/k^2$ was previously established by minimization considerations [32,36,47]. There seems to be a total interface thickness kt -dependent coefficient from our simulations, namely, $1 + (\pi/2 - 1) \cos(\pi kt/2)^2$, a decreasing function of the interface number k as well for kt between 0 and 1. Hence, from Eq. (32), the inhomogeneity energy e_{inh} favors microstructures with large interface numbers, in contrast to the interface energy of Eq. (31). Therefore, a proper number of interfaces would be selected by the combination of both interface and inhomogeneity energies.

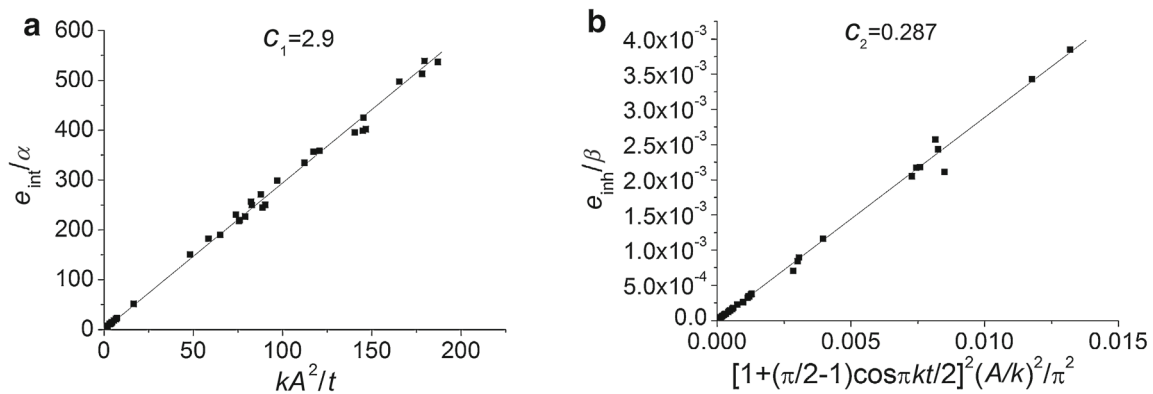


Fig. 9 Energies of inhomogeneous solutions with different interface numbers, at various loadings and for several parameters. **a** Interface energy. **b** Inhomogeneity energy

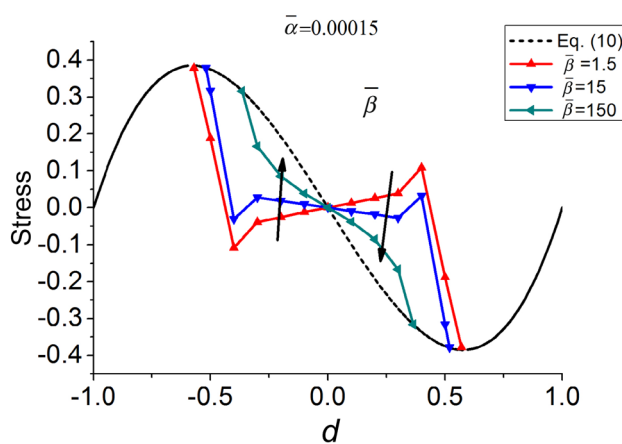


Fig. 10 Stress–strain curve

The stress field is also worth paying attention to. The stress field should satisfy the divergence-free condition in mechanical equilibrium. Therefore, in our one-dimensional model, the stress should be a constant along the specimen. Although the strain field fluctuates between the two phases as a function of positions along the specimen, the contributions of the interface and constraint energy upon the stress balance the fluctuation of the elastic energy along the specimen, thereby keeping the stress constant. The stress–strain relation is nonmonotonic (Fig. 10) and is, moreover, nonunique for LEMs. A unique stress–strain curve can be obtained if global energy minimization is considered. Under global energy minimization, each set of material parameters gives its unique stress–strain curve (Fig. 10). The hysteresis is influenced by the two material parameters α and β . When α or β is small, the stress jumps down at strain $-\varepsilon_0$ then increases with the strain, and finally jumps down again at ε_0 ; when α or β is large, the stress jumps down at strain $-\varepsilon_0$ and ε_0 but does not see any rise against the strain (though only changing β is shown in Fig. 10). The dynamic effects would need

to be considered if this were being compared with experiments.

5 Conclusions

Microstructures of fine mixtures are obtained as the local energy minimizers of a one-dimensional nonlinear elastic model with a foundation energy that mimics the constraint energy imposed on boundaries and surrounding matrix. The minimizers are inhomogeneous solutions of the nonlinear Euler–Lagrange equation of the total energy functional. Both the conditions for the appearance of such solutions and the numerical solutions are obtained and analyzed.

The bifurcation condition for the appearance of inhomogeneous solutions can be obtained through either local bifurcation analysis or homotopy analysis. The condition defines a region in the loading–interface number plane, in which inhomogeneous solutions may appear as metastable states and a trivial homogeneous solution becomes unstable. Multiple bifurcations to solutions with varying numbers of interfaces can occur during the loading–unloading process. Both the geometrical and material properties strongly influence the bifurcation condition.

Numerical solutions with large numbers of interfaces can be obtained using the proposed hybrid method, which combines homotopy analysis with the FDM. In addition to the interface number, the solutions of phase mixtures must be characterized by the interface thickness and the strain amplitudes. Approximated analytical expressions are obtained for the interface and inhomogeneity energies. They indicate clearly that both energies are completely determined by three parameters: the interface number, the interface thickness, and the strain amplitude. Thus, we may call them the characteristic parameters of the LEMs.

Acknowledgments This project was supported by the National Natural Science Foundation of China (Grants 11461161008 and 11272092).

References

1. Kaufman, L., Cohen, M.: Martensitic transformations. In: Chalmers, B., King, R. (eds.) *Progress in Metal Physics*, vol. 7, 165–246. Pergamon Press, Oxford (1958)
2. Nishiyama, M.: *Transformations*. Academic Press, San Diego (1978)
3. Olson, G.B., Cohen, M.: Thermoelastic behavior in martensitic transformations. *Scripta Met.* **9**, 1247–1254 (1975)
4. Duerig, T.W., Melton, K.N., Stöckel, D.: *Engineering Aspects of Shape Memory Alloys*. Butterworth-Heinemann, London (1990)
5. Otsuka, K., Wayman, C.M.: *Shape Memory Materials*. Cambridge University Press, Cambridge (1999)
6. Wu, Z.Q., Zhang, Z.H.: Force-displacement characteristics of simply supported beam laminated with shape memory alloys. *Acta Mechanica Sinica* **27**, 1065–1070 (2011)
7. Yang, S.B., Xu, M.: Finite element analysis of 2D SMA beam bending. *Acta Mechanica Sinica* **27**, 738–748 (2011)
8. Rong, Q.Q., Cui, Y.H., Shimada, T., et al.: Self-shaping of bio-inspired chiral composites. *Acta Mechanica Sinica* **30**, 533–539 (2014)
9. Bhattacharya, K.: *Microstructure of Martensite*. Oxford University Press, Oxford (2003)
10. Cheng, P., Xingyao, W., Yongzhong, H.: Characteristics of stress-induced transformation and microstructure evolution in Cu-based SMA. *Acta Mechanica Solida Sinica* **21**, 1–8 (2008)
11. Roubicek, T.: Models of microstructure evolution in shape memory alloys. In: Ponte Castaneda, P., et al. (eds.) *Nonlinear Homogenisation and Its Applications to Composites, Polycrystals and Smart Materials*, 269–304. Kluwer Academic publishers, Dordrecht (2004)
12. Patoor, E., Lagoudas, D.C., Entchev, P.B., et al.: Shape memory alloys, Part I: general properties and modeling of single crystals. *Mech. Mater.* **38**, 391–429 (2006)
13. Lagoudas, D.C., Entchev, P.B., Popov, P., Patoor, E., Brinson, L.Catherine, Gao, Xiujie., et al.: Shape memory alloys, Part II: modeling of polycrystals. *Mech. Mater.* **38**, 430–462 (2006)
14. Porta, M., Lookman, T.: Heterogeneity and phase transformation in materials : energy minimization, iterative methods and geometric nonlinearity. *Acta Materialia* **61**, 5311–5340 (2013)
15. Cesana, P., Porta, M., Lookman, T.: Asymptotic analysis of hierarchical martensitic microstructure. *J. Mech. Phys. Solids* **72**, 174–192 (2014)
16. Guquan, S., Qingping, S., Kehchih, H.: Effect of microstructure on the hardening and softening behaviors of polycrystalline shape memory alloys Part I: Micromechanics constitutive modeling. *Acta Mechanica Sinica* **16**, 309–324 (2000)
17. Xiangyang, Z., Qingping, S., Shouwen, Y.: On the strain jump in shape memory alloys—a crystallographic-based mechanics analysis. *Acta Mechanica Sinica* **15**, 134–144 (1999)
18. Li, J.Y., Lei, C.H., Li, L.J., et al.: Unconventional phase field simulations of transforming materials with evolving microstructures. *Acta Mechanica Sinica* **28**, 915–927 (2012)
19. Maxwell, J.C., Lord, Rayleigh: *Encyclopedia Britannica* (1876)
20. Christian, J.W.: *The Theory of Transformations in Metals and Alloys*. Pergamon Press, New York (2002)
21. Khachaturyan, A.G.: *Theory of Structural Transformations in Solids*. John Wiley & Sons, New York (1983)
22. Mueller, I., Seelecke, S.: Thermodynamic aspects of shape memory alloys. *Math. Comput. Model* **34**, 1307–1355 (2001)
23. Yan, Y., Yin, H., Sun, Q.P., et al.: Rate dependence of temperature fields and energy dissipations in non-static pseudoelasticity. *Contin. Mech. Thermodyn.* **24**, 675–695 (2012)
24. Yin, H., Yan, Y., Huo, Y.Z., et al.: Rate dependent damping of single crystal CuAlNi shape memory alloy. *Mater. Lett.* **109**, 287–290 (2013)
25. Hao, Yin, Yongjun, He, Qingping, Sun: Effect of deformation frequency on temperature and stress oscillations in cyclic phase transition of NiTi shape memory alloy. *J. Mech. Phys. Solids* **67**, 100–128 (2014)
26. Shield, T.W.: Orientation dependence of the pseudoelastic behaviour of single crystals of Cu–Al–Ni in tension. *J. Mech. Phys. Solids* **43**, 869–895 (1995)
27. Waitz, T., Antretter, T., Fischerb, F.D., et al.: Size effects on the martensitic phase transformation of NiTi nanograins. *J. Mech. Phys. Solids* **55**, 419–444 (2007)
28. Ueland, S.M., Schuh, C.A.: Transition from many domain to single domain martensite morphology in small-scale shape memory alloys. *Acta Materialia* **61**, 5618–5625 (2013)
29. Sun, Q.P., Aslan, A., Li, M.P., et al.: Effects of grain size on phase transition behavior of nanocrystalline shape memory alloys. *Sci. China Technol. Sci.* **57**, 671–679 (2014)
30. Ericksen, J.L.: Equilibrium of bars. *J. Elast.* **5**, 191–202 (1975)
31. Carr, J., Gurtin, M.E., Slemrod, M.: Structured phase transition on a finite interval. *Arch. Rat. Mech. Anal.* **86**, 317–351 (1984)
32. Müller, S.: Singular perturbations as a selection criterion for periodic minimizing sequences. *Cal. Var. Partial Diff. Equ.* **1**, 169–204 (1993)
33. Truskinovsky, L., Zanzotto, G.: Ericksen’s bar revisited: energy wiggles. *J. Mech. Phys. Solids* **44**, 1371–1408 (1996)
34. Vainchtein, A., Healey, T., Rosakis, P., et al.: The role of the spinodal in one dimensional phase transitions microstructures. *Phys. Rev. D.* **115**, 29–48 (1998)
35. Anna, V., Healey, T.J., Rosakis, P.: Bifurcation and metastability in a new one-dimensional model for martensitic phase transitions. *Comput. Methods Appl. Mech. Eng.* **170**, 407–421 (1999)
36. Ren, X., Truskinovsky, L.: Finite scale microstructures in nonlocal elasticity. *J. Elast.* **59**, 319–355 (2000)
37. Vainchtein, A.: Dynamics of phase transitions and hysteresis in a viscoelastic Ericksen’s bar on an elastic foundation. *J. Elast.* **57**, 243–280 (1999)
38. Vainchtein, A.: Hysteresis and stick-slip motion of phase boundaries in dynamic models of phase transitions. *J. Nonlinear Sci.* **9**, 697–719 (1999)
39. Xuan, C., Peng, C., Huo, Y.: One dimensional model of Martensitic transformation solved by Homotopy analysis method. *Z. Naturforsch* **67a**, 230–238 (2012)
40. Liao, S.J.: *Beyond Perturbation: Introduction to the Homotopy Analysis Method*. Chapman & Hall/ CRC, Boca Raton (2003)
41. Liao, S.: *Homotopy Analysis Method in Nonlinear Differential Equations*. Higher education press, Beijing (2011)
42. Wechsler, M., Lieberman, D., Read, T.: On the theory of the formation of martensite. *Trans. AIME J. Metals* **179**, 1503–1515 (1953)
43. Bowles, J., MacKenzie, J.: The crystallography of martensitic transformations I and II. *Acta Metal. Mater.* **2**, 129–147 (1954)
44. Santman, S., Guo, Z.: Large shearing oscillations of incompressible nonlinear elastic. *J. Elast.* **14**, 249–262 (1984)
45. Ball, J.M., James, R.D.: Fine phase mixtures as minimizers of energy. *Arch. Rat. Mech. Anal.* **100**, 13–52 (1987)
46. Kohn, R., Müller, S.: Surface energy and microstructure in coherent phase transitions. *Comm. Pure. Appl. Math.* **47**, 405–435 (1994)
47. Huo, Y., Muller, I.: Interfacial and inhomogeneity penalties in phase transitions. *Contin. Mech. Thermodyn.* **15**, 395–407 (2003)
48. Hui-Hui, D., Zongxi, C.: An analytical study on the instability phenomena during the phase transitions in a thin strip under uniaxial tension. *J. Mech. Phys. Solids* **60**, 691–710 (2012)
49. Kalies, W.: Regularized models of phase transformation in one-dimensional nonlinear elasticity. [Ph. D. Thesis], Cornell University (1994)